Acta Crystallographica Section A
Foundations of Crystallography
ISSN 0108-7673

Received 9 April 2004
Accepted 14 July 2004

The local form of the source function as a fingerprint of strong and weak intra- and intermolecular interactions

Carlo Gatti* and Luca Bertini

CNR–ISTM Istituto di Scienze e Tecnologie Molecolari, via Golgi 19, 20133 Milan, Italy.
Correspondence e-mail: c.gatti@istm.cnr.it

This work introduces a local form for the source function, from each atom, for the electron-density value at a given point. The source function enables one to equate the value of the electron density at any point within a molecule to a sum of atomic contributions and thus to view properties of the density at representative points, such as the bond critical points, from a new perspective. The local form of the function introduces further detail. When plotted along a bond path and with reference to the bond critical point (b.c.p.), the source function shows which regions of the atoms involved in the bonding are accumulating or removing electronic charge at the b.c.p. The local form of the source function therefore represents an interesting fingerprint of a given bonding interaction. The local source may be expressed as a sum of two contributions, related to the kinetic energy density and electronic potential energy density, respectively. This approach gives further physical insight into why an atomic region is accumulating or removing charge at the b.c.p. The local form of the source function is applied to the study of the second-row diatomic hydride series and of a number of prototypical hydrogen-bonded systems. Differences in the local source contributions to the density at bond critical points due to chemical bonding (deformation density) and crystallization (interaction density) are also explored and found to be more informative and experimentally detectable than are the corresponding changes for the bond-critical-point properties of weak intermolecular interactions. This result might be of potential interest when judging the data quality of a charge-density experimental determination. Although the present paper deals with electron densities derived from theoretical computations only, both the source function and its local form should also be easily obtainable from a charge-density quality X-ray diffraction experiment.

1. Introduction

A few years ago, Bader & Gatti (1998) showed that it is possible to view the electron density ρ at any point $\mathbf{r}$ within a molecule as consisting of contributions from a local source operating at all other points $\mathbf{r}'$. If this local source is evaluated over regions Ω bounded by surfaces $S_\Omega(\mathbf{r})$ that satisfy the topological definition of an atom (Bader, 1990), the density at $\mathbf{r}$ may be equated to a sum of atomic contributions $S(\mathbf{r}, \Omega)$, each of which is termed as the *source function* from atom Ω to $\rho(\mathbf{r})$. We can then envisage the density within an atom as being determined solely by an internal source function (SF) self-contribution and by SF contributions from the remaining atoms or groups of atoms within the molecule. Such decomposition enables us to view the properties of the density from a new perspective and establishes the SF as a novel interesting tool for providing chemical insight. Few applications of this function have, however, appeared up to now.

Bader & Gatti (1998) suggested that the SF should be useful in studying the consequences of the transferability of the properties of a functional group. Indeed, the extent of transferability of these properties from one molecule to another involves not only a corresponding transferability of the group's electron density but also a constancy of the sum of contributions to this density from the remaining atoms or groups of atoms in the system. For example, it was shown that the characteristic density at the bond critical point (b.c.p.) for the unique terminal C—H bond in a hydrocarbon chain requires that the contribution to the density from atomic sources outside the group remains constant, regardless of the length of the chain. A second study (Overgaard *et al.*, 2001) used the SF tool in a charge-density study of the strong

hydrogen bonds in a model compound of the catalytic triad in serine proteases. This study showed that the SF might constitute a sensitive measure for the nature of a hydrogen bond. Comparison between a low-barrier (Cleland & Krevoy, 1994) (benzoylacetone) and a single-well (nitromalonamide) hydrogen-bonded system indicated that the low-barrier hydrogen-bonded state is characterized by a much larger source contribution from the H atom to the density at the hydrogen-bond critical point (c.p.), despite the similar O···O separations. The difference between the two systems was shown to arise from the very different shape of their Laplacian distribution in the H···O region, which yields very different SFs from the corresponding H atoms at the hydrogen-bond c.p. The challenging study of Overgaard *et al.* (2001) called for further investigations, as it covered only a very small range of the donor–acceptor separations found in hydrogen bonds. A third paper, by Gatti *et al.* (2003), demonstrated that the SF enables the classification of hydrogen bonds in terms of characteristic SF contributions to the density at the hydrogen-bond c.p. from the H atom involved in the hydrogen bond, from the H-atom donor *D* and from the H-atom acceptor *A*. The five hydrogen-bond classes defined by Gilli & Gilli (2000) using chemical and geometrical considerations have distinctive quantitative features in terms of the SF. The source contribution from the H atom appears as the most characteristic marker of the hydrogen-bond strength, being highly negative for isolated hydrogen bonds, slightly negative for polarized assisted hydrogen bonds, close to zero for resonance-assisted hydrogen bonds and largely positive for charge-assisted hydrogen bonds. The contributions from atoms other than H, *D* and *A* were found to increase strongly with decreasing hydrogen-bond strength, consistent with the parallel increased electrostatic character of the interaction. The study of Gatti *et al.* (2003) also highlighted a correspondence between the classification of hydrogen bonds given by the SF and by the electron localization function topological approach (Fuster & Silvi, 2000). Further examples of the use of the SF were shown in the paper, including the bond nature in the second-row H*X* diatomic species with changing *X*, the extent of transferability of the Li basin in the Li*X* (*X* = F, O, N, Cl and H) series and the non-local origin of non-nuclear attractors (Gatti *et al.*, 1987) in lithium clusters. On the basis of all these applications, it was concluded (Gatti *et al.*, 2003) that the SF represents a practical tool for disclosing the local and non-local character of the electron-density distributions, since the SF quantifies such a locality and non-locality in terms of a chemically appealing and physically sound partitioning. The use of the SF tool is not restricted to theoretical studies. Indeed, it requires the knowledge of only the system's electron density (and derivatives) and not of the system's wavefunction, despite the fact that this tool is providing access to non-local information. The SF is thus also easily obtainable from a charge-density quality X-ray diffraction experiment.

Although further work would be required to explore the chemical insight that may be derived from the SF tool as used so far, the present paper has a different target and is aimed at investigating whether the *local source* contributions to the density at a point are interesting in their own right. The local source may be expressed as a sum of two terms, one related to the local kinetic energy and the other to the local electron potential energy. We evaluate the local contributions from the whole space to the bond density in a series of systems, using the b.c.p. as the least biased choice for the reference point associated with a bond. We also examine whether these local contributions to the b.c.p. density are a more distinctive marker of the electron-density rearrangements due to chemical bonding (deformation density) and crystallization (interaction density) than are the corresponding changes observed at b.c.p.s of weak intermolecular interactions. This question might be of potential interest when judging the data quality of a charge-density experimental determination.

2. Theory

2.1. The local source and the source function

Bader & Gatti (1998) showed that, for a closed system with boundaries at infinity, equation (1) gives the density at a point $\mathbf{r}$ within an atomic basin Ω:

$$\rho(\mathbf{r}) = \int \mathrm{LS}(\mathbf{r}, \mathbf{r}')\,\mathrm{d}\mathbf{r}' = \int_{\Omega} \mathrm{LS}(\mathbf{r}, \mathbf{r}')\,\mathrm{d}\mathbf{r}' + \sum_{\Omega' \neq \Omega} \int_{\Omega'} \mathrm{LS}(\mathbf{r}, \mathbf{r}')\,\mathrm{d}\mathbf{r}'. \quad (1)$$

The right-hand side of the equation is an integral over the whole space of a local source $\mathrm{LS}(\mathbf{r}, \mathbf{r}')$ for the density at $\mathbf{r}$, which may be decomposed as a sum of an internal self-contribution from the basin Ω and a contribution from the remaining basins in the system. The local source is defined as[1]

$$\mathrm{LS}(\mathbf{r}, \mathbf{r}') = -(1/4\pi)\,\nabla^2\rho(\mathbf{r}')/|\mathbf{r} - \mathbf{r}'|, \quad (2)$$

where $(4\pi|\mathbf{r} - \mathbf{r}'|)^{-1}$, a Green's function, may be seen (Arfken, 1985) as an *influence function* representing the effectiveness of how the *cause* $\nabla^2\rho(\mathbf{r}')$ gives rise to the *effect* $\rho(\mathbf{r})$. The effectiveness of the Laplacian of the density in producing the electron distribution depends on the distance between the element of Laplacian of the density $\nabla^2\rho(\mathbf{r}')\,\mathrm{d}\mathbf{r}'$ and the point of interest given by $\mathbf{r}$. Calling the integral over a basin Ω of the local source for the density at $\mathbf{r}$ the *source function* from Ω, $S(\mathbf{r}, \Omega)$,

$$\int_{\Omega} \mathrm{LS}(\mathbf{r}, \mathbf{r}')\,\mathrm{d}\mathbf{r}' \equiv S(\mathbf{r}, \Omega), \quad (3)$$

the electron density at $\mathbf{r}$ within an atom is given by a source function internal to the atom and by a source function from each of the remaining atoms in the total system:

$$\rho(\mathbf{r}) = S(\mathbf{r}, \Omega) + \sum_{\Omega' \neq \Omega} S(\mathbf{r}, \Omega'). \quad (4)$$

This function is thus a measure of the relative importance of an atom's or a group's contribution to the density at any point.

[1] At variance with Bader & Gatti (1998), the term $-1/(4\pi)$ is here included in the definition of the local source.

2.2. The local source components

The Laplacian also appears (Bader, 1990) in the local expression of the virial theorem,

$$\nabla^2\rho(\mathbf{r}) = (4m/\hbar^2)[2G(\mathbf{r}) + V(\mathbf{r})], \quad (5)$$

and the local source is thus related to the failure to satisfy locally the virial relationship between twice the positively defined kinetic energy density, G, and the virial or electronic potential energy density, V:

$$\mathrm{LS}(\mathbf{r}, \mathbf{r}') = -(m/\pi\hbar^2)[2G(\mathbf{r}) + V(\mathbf{r})]/|\mathbf{r} - \mathbf{r}'|. \quad (6)$$

It is therefore possible to express the local source in terms of a local kinetic energy LG and a local electron potential energy LV source contribution:[2]

$$\mathrm{LS}(\mathbf{r}, \mathbf{r}') = \mathrm{LG}(\mathbf{r}, \mathbf{r}') + \mathrm{LV}(\mathbf{r}, \mathbf{r}'), \quad (7)$$

$$\mathrm{LG}(\mathbf{r}, \mathbf{r}') = -(m/\pi\hbar^2)2G(\mathbf{r})/|\mathbf{r} - \mathbf{r}'|, \quad (8)$$

$$\mathrm{LV}(\mathbf{r}, \mathbf{r}') = -(m/\pi\hbar^2)V(\mathbf{r})/|\mathbf{r} - \mathbf{r}'|. \quad (9)$$

LG always gives a negative contribution to the density at $\mathbf{r}$ since G is everywhere positive, while the opposite holds true for LV, V being everywhere negative. Hence the regions in a system where the electron density is concentrated [$\nabla^2\rho(\mathbf{r}) < 0$] and the potential energy dominates over the kinetic energy are a source for the electron density at a point $\mathbf{r}'$, while regions where the electron density is depleted [$\nabla^2\rho(\mathbf{r}) > 0$] and where the kinetic energy dominates over the potential energy act as a sink for $\rho(r)$. The effectiveness of the electron density at $\mathbf{r}$ as a source or a sink for the electron density at another point $\mathbf{r}'$ is then related to the magnitude of the charge concentration or depletion at $\mathbf{r}$, weighted by the inverse of the distance of the two points.

Contrary to the situation for the local source, the LG and LV contributions are not directly amenable to experimental determination. However, they can be estimated either from a wavefunction constrained to experiment (Jayatilaka & Grimwood, 2001) or by inserting into (8) and (9) the approximate expression for $G(\mathbf{r})$ proposed by Abramov (1997) and the value of V that is obtained from the local form of the virial theorem [equation (5)] using the approximate G value.

3. Computational details

3.1. Evaluation of the local source contributions

The *AIMPAC* (McMaster University, 1997) and *TOPOND98* (Gatti, 1999) codes were modified in order to evaluate LS, LG and LV along a bond path or a line. Modified *AIMPAC* and *TOPOND98* codes were used for gas-phase and crystalline systems, respectively. If a b.c.p. between two atoms is used as the reference point, the modified codes automatically locate the requested b.c.p. The codes then evaluate the associated bond path and the LS, LG and LV contributions to the density at b.c.p. along this path. Code has also been written to handle the case of the juxtaposition of two bond paths or lines, using the output from either *AIMPAC* or *TOPOND98*. For the sake of simplicity and of using a single numerical scale for the profiles of the electron density, the Laplacian $\nabla^2\rho$, LS, LG and LV along a bond path/line, atomic units (a.u.) were adopted throughout the paper. This approach implies $m = 1$ and $\hbar = 1$ in equations (5)–(9). LS, LG and LV when multiplied by a volume element $\mathrm{d}\mathbf{r}'$ have the same dimension as $\rho(r)$, with 1 a.u. of electron density corresponding to 6.74834 e Å^{-3}. A value of $\nabla^2\rho(r) = 1$ a.u. corresponds to 24.09879 e Å^{-5}. When comparing bonding interactions along a series, profiles of the quantities above, along an $A-B$ bond path, were evaluated against a dimensionless parameter t, with $t = 0$ at nucleus A, $t = 1$ at nucleus B and a step size equal to 0.005 (201 points per line). Values along profiles were cut using a threshold of 5 a.u. for the electron density and 10 a.u. for LS, LG, LV and $\nabla^2\rho(r)$. This approach automatically removes from the plots uninteresting information too close to the nuclei, except for the H nucleus.[3] The electron density and $\nabla^2\rho(r)$ values at the b.c.p. were added to the list of points evaluated along a line, whilst the corresponding LS, LG and LV values were not inserted, in order to avoid singularities [see equations (2), (8) and (9)].

3.2. Investigated systems

The adopted level of calculation is not the best that may be used on the investigated systems, but it should be good enough for a qualitative insight into the information that may be obtained from the local form of the source function. Unless otherwise stated, we adopted the wavefunctions employed by Gatti *et al.* (2003) for evaluating the source contributions condensed to atoms (the source functions). This approach enables us to compare information from the local and the integral contributions to the density when necessary.

3.2.1. Second-row diatomic hydrides. Wavefunctions for HX systems (X = Li, Be, B, C, N, O, F and H) were taken from a previous study (Hô *et al.*, 1998) that used the CISD (configuration interaction with single and double excitations) method, the 6-31G basis set (Frisch *et al.*, 1998), and the experimental geometry and the ground-state electron configuration both from Huber & Herzberg (1979). This set of wavefunctions was computed with *GAUSSIAN98* (Frisch *et al.*, 1998).

3.2.2. Hydrogen-bonded systems. The wavefunctions for prototypical hydrogen-bonded systems were taken from our previous source function study (Gatti *et al.*, 2003), which adopted a B3LYP/6-31G(d,p)//B3LYP/6-31G(d,p) computational level (Frisch *et al.*, 1998). Contrary to previous work, we also adopted this level of theory for the water dimer. This approach has the disadvantage of giving a poor estimate for the donor-to-acceptor separation in this complex [2.88 Å, to be compared with the experimental value of 2.98 (3) Å (Dyke *et al.*, 1977)] but the obvious advantage of allowing an unbiased comparison of the local source profiles among the

[2] The local source could also be expressed in terms of local contributions related to the total electronic energy density $H(\mathbf{r})$ (Cremer & Kraka, 1984) and to the kinetic energy density $G(\mathbf{r})$, since, in atomic units, $\nabla^2\rho = 4[2G(\mathbf{r}) + V(\mathbf{r})] = 4[G(\mathbf{r}) + H(\mathbf{r})]$.

[3] We classify information as uninteresting when it would be indistinguishable from the case of an isolated atom.

various hydrogen-bonded systems. The integrated source-function values for the water dimer have been recomputed accordingly and differ significantly from those published previously (Gatti *et al.*, 2003) owing to the noteworthy decrease of the donor-to-acceptor distance (from 3.020 to 2.876 Å).

According to the general classification and nomenclature of hydrogen bonds proposed by Gilli & Gilli (2000), we investigated the following prototypical cases, listed in order of decreasing hydrogen-bond strength and hereinafter identified by their roman number in bold.

I. The symmetrical $H_5O_2^+$ species as a case (Fuster & Silvi, 2000) of a positive charge-assisted hydrogen bond, +CAHB.

II. The open form of the formic acid–formate anion complex (Pan & McAllister, 1997) as an example of a negative charge-assisted hydrogen bond, −CAHB.

III. Malonaldehyde, which is a typical resonance-assisted hydrogen bond, RAHB.

IV. The cyclic homodromic (Jeffrey, 1997) water trimer (Mó *et al.*, 1992) as a case of a polarization-assisted hydrogen bond, PAHB.

V. The water dimer, as an example of an isolated hydrogen bond, IHB, of moderate strength.

VI. The water–acetylene complex (Turi & Dannenberg, 1993) as a case of a moderately weak IHB.

Symmetry constraints were C_{2h} for **I**, C_1 for **IV**, and C_s for **II**, **III**, **V** and **VI**.

3.2.3. Urea crystal. The crystal structure of urea was taken from the 12 K neutron data of Swaminathan *et al.* (1984). The basis set (6-31G**) used in the previous study (Gatti *et al.*, 1994) of the crystal field effects on the topological properties of the electron density in urea was adopted in the *CRYSTAL98* (Saunders *et al.*, 1998) calculation. The electron density and the local source contributions for the cases of the independent atom model (IAM; Coppens, 1997) and of the non-interacting molecules in the crystal were evaluated by using the *PATO* and *MOLSPLIT* options of *CRYSTAL98*, respectively. The associated density matrices were then provided to the modified *TOPOND98* code. The basis set and geometry used for the evaluation of the wavefunction for the crystal was adopted. This approach enabled us to evaluate the local source contributions for the *deformation density* (crystal density *minus* the superposition of atomic densities of atoms placed as in the crystal) and the *interaction density* (crystal density *minus* the superposition of the density of isolated molecules placed at the same locations as in the crystal).

4. Results and discussion

We evaluated the local contributions to the bond density in a series of systems. This process requires an arbitrary choice of the reference point associated with a bond $A-B$. We used the b.c.p. as the least biased choice. Indeed, this is a point where $\nabla\rho$ vanishes and which does not belong exclusively to either of the two bonded atoms since it lies on their interatomic surface. Furthermore, it is the point on the $A-B$ interatomic surface that has the highest density value and the minimal distance from the A and B nuclei. For the case of deformation and interaction densities, the b.c.p. of the crystal density was taken as a reference point.

We have then to choose where the source contributions to the density at the b.c.p. are to be computed and analysed. For a covalent bond $A-B$, it has been found (Gatti *et al.*, 2003) that the sum of the source function contributions from A and B amounts to about 90–95% of the value of the density at the b.c.p. In this case, the remaining atoms in the molecule are providing very small or even negligible source function contributions to the $A-B$ b.c.p., although the local source contributions within their basins are not negligible. This situation is the result of a nearly perfect balance between the positive and negative local source contributions when integrated over the basin volume. For an intermolecular interaction, more atoms come into the play. For instance, we showed that the sum of the source contributions to the density at the hydrogen-bond c.p. from the H atom, the H-atom donor D and the H-atom acceptor A ranges from ∼40 to ∼90%, according to the nature of the hydrogen bond (Gatti *et al.*, 2003). Therefore, we have evaluated the local source function contribution along the $A-B$ bond path for diatomic species and along the juxtaposition of the $D-$H and H$\cdots A$ bond paths for hydrogen-bonded systems. Once again, selecting the bond path seemed to us to be the less biased choice, since this is the line joining the two nuclei that has maximum density with respect to any lateral displacement from the line. In other words, we chose the points along the bond path (or along two juxtaposed bond paths for hydrogen-bonded systems) as the most representative of the charge-density rearrangements and hence of local source contribution changes, due to bonding. While this assumption appears reasonable for the investigated systems, it is however an arbitrary one and different choices could be invoked in other cases. For instance, non-bonding regions (lone pairs) play an important role in several bonding patterns. These regions could be examined either as a significant source for the electron density at their neighbouring b.c.p.s or as areas where source/sink contributions from the remaining molecular space would be worth investigating.

4.1. Second-row hydrides, H*X*

Fig. 1 displays profiles for the electron density, its Laplacian, and the local source contributions LS, LG and LV for the eight hydrides (HH was also included as a case with equal electronegativity for H and X, thus having symmetric profiles for all quantities with respect to the b.c.p.). Profiles are reported as a function of the dimensionless parameter t, with the H atom at $t = 0$. For each system, the interval $(t_{\rm b.c.p.} - 0.2) \leq t \leq (t_{\rm b.c.p.} + 0.2)$ is shown, and the electron density is multiplied by a factor of 5 so as to report all quantities on the same scale. Table 1 lists various properties at the b.c.p. and the source contribution from the H atom to the electron density at the b.c.p.

Let us first consider the general trends for each displayed function. In the reported interval for t, the electron density is indeed a slowly varying function as it increases by no more

than 10–20% with respect to the value at the b.c.p. The value at the b.c.p. (Table 1) increases with increasing *X*-atom electronegativity, and this behaviour differentiates one interaction from another in terms of the electron density. The Laplacian varies more significantly and its profile denotes more clearly the kind of bond. The Laplacian is everywhere positive over the plotted interval for HLi, while it is everywhere negative in the H*X* series past HB, with the most negative side being that

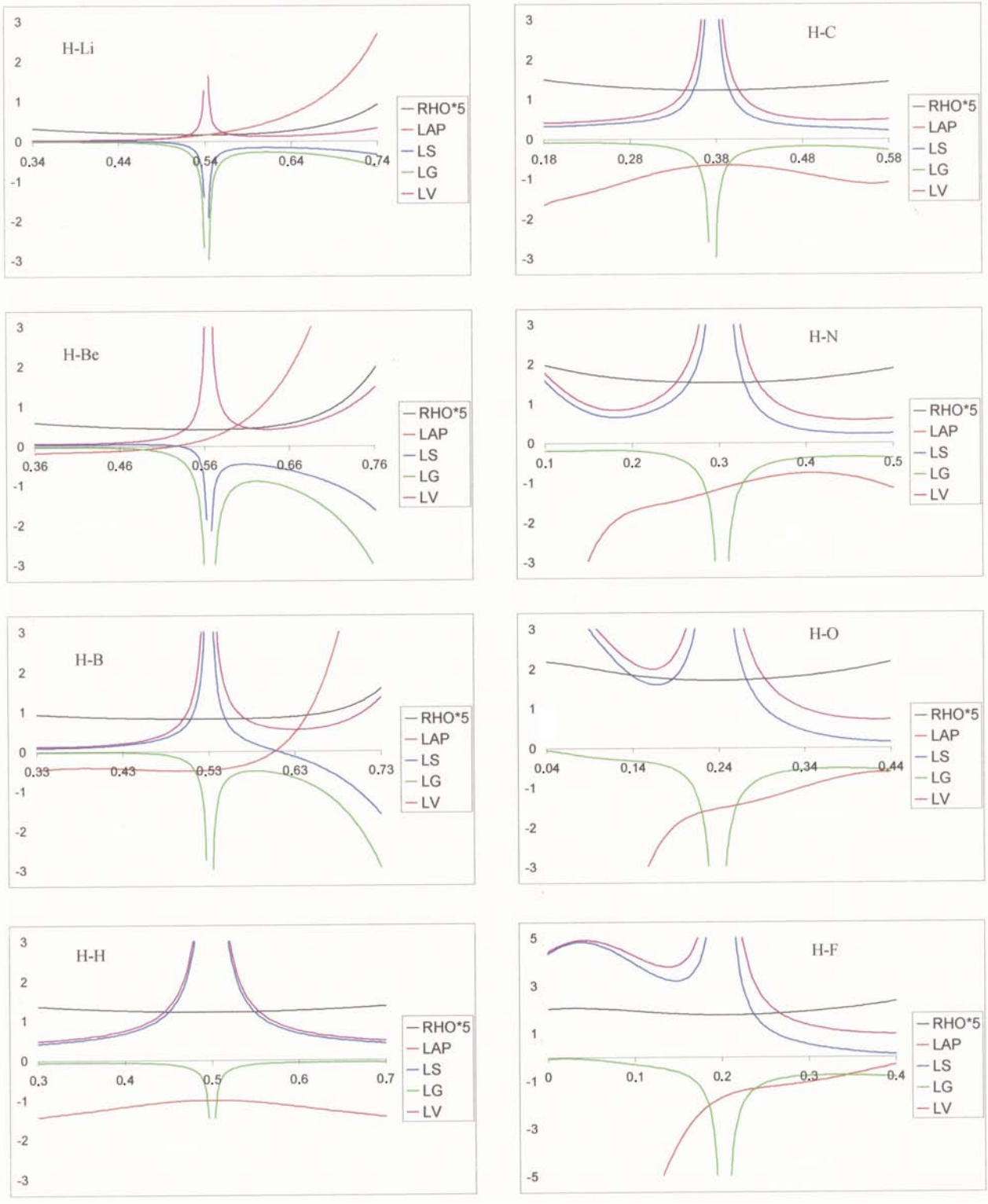

Figure 1
Second row-hydrides, H*X*. The local source contribution (LS) to the density at the b.c.p. from points lying on the bond path ($t = 0$ at the H nucleus and $t = 1$ at the *X* nucleus). The LG and LV components of LS and the profiles of the electron density (RHO) and Laplacian (LAP) are also reported. RHO is multiplied by 5 and all quantities are in a.u. (see text).

Table 1
Second-row hydrides: properties and source function contributions at the b.c.p. and H-atom electron population.

All quantities are in a.u. unless otherwise stated. H*X* systems are listed in order of increasing ρ(b.c.p.) value.

H*X*	R_e (Å)	ρ(b.c.p.)†	$\nabla^2\rho$(b.c.p.)	G(b.c.p.)	V(b.c.p.)	S(b.c.p., H) (%)†‡	N(H)†§
HLi ($^1\Sigma^+$)	1.596	0.033	0.155	0.036	−0.034	0.020 (60.1)	1.874
HBe ($^2\Sigma^+$)	1.343	0.083	0.188	0.078	−0.108	0.050 (60.3)	1.798
HB ($^1\Sigma^+$)	1.232	0.163	−0.488	0.039	−0.200	0.085 (52.2)	1.574
HH ($^1\Sigma_g^+$)	0.741	0.243	−1.012	0.012	−0.276	0.122 (50.0)	1.000
HC ($^2\Pi$)	1.120	0.245	−0.664	0.038	−0.242	0.110 (44.8)	1.052
HN ($^3\Sigma^-$)	1.036	0.305	−1.161	0.070	−0.430	0.132 (43.2)	0.781
HO ($^2\Pi$)	0.970	0.340	−1.548	0.087	−0.561	0.140 (41.0)	0.550
HF ($^1\Sigma^+$)	0.917	0.354	−1.686	0.104	−0.629	0.137 (38.8)	0.399

† Gatti *et al.* (2003). ‡ Percentage source contributions to ρ(b.c.p.) are reported in parentheses. § H-atom electron population.

closer to the H atom. For HBe and HB, the Laplacian changes its sign with increasing t and becomes positive just before the b.c.p. in HBe and largely after the b.c.p. in HB. These results are more clearly understood by looking at the contour maps of the Laplacians of these systems. As shown in Fig. 1 of Gatti *et al.* (2003), starting from HLi and ending at HF, the b.c.p. moves from a region of positive Laplacian closer to *X* to a region of negative Laplacian, shared between the two atoms, closer to the H nucleus. Transition from a closed-shell to shared atomic interactions and from a hydride ion in HLi to cationic H in HF [see the H electron populations N(H) in Table 1] is well depicted by the whole Laplacian distribution.

The ionic character of a non-shared interaction, or the departure from covalency of a shared H—*X* interaction, is also nicely represented by the asymmetry of the Laplacian profile (Fig. 1) with respect to the b.c.p. The H—H interaction is obviously perfectly symmetric. Asymmetry increases from H—C to H—F, with increasing net negative or net positive charge on the H atom (Table 1), according to the increased polarity of the bond. The same holds true from H—B to H—Li, with the Laplacian changing sign somewhere along the interval, the interactions in these diatomic species being non-shared or quasi-non-shared.

Now the question arises of what is the main difference between the Laplacian and the LS profile, since the latter is defined in terms of the first. Basically, the difference is that the LS profile explicitly relates the Laplacian of the density at a point along the bond path to the value of the electron density at what is reckoned as the most representative point of a chemical interaction. It is non-local information, relating a property at the b.c.p. to properties at an infinite set of points distinct from the b.c.p. In practice, what additional chemical information is provided by the profiles of the local source and of its LG and LV contributions? Firstly, the LS profile indicates whether a point along the bond path is acting as a source or a sink for the density at the b.c.p. and the magnitude of such a contribution. Secondly, LG and LV profiles and their differences give a physical rationalization of why a point along the bond path is acting as a source rather than as a sink, and why it is more or less effective in doing so. The LS profiles for the H—Li and H—Be interactions show that the regions around the b.c.p. act as a modest sink for the density at the b.c.p., in agreement with the non-shared character of these interactions. The H—B interaction represents a borderline situation, with the source being everywhere positive on the H-atom side and becoming negative $0.1t$ from the b.c.p. on the B-atom side, in obvious agreement with the change of the sign of the Laplacian. For the other hydrides, having shared interactions, the regions around the b.c.p. act as sources with contributions whose importance rises with increasing charge density at the b.c.p. More importantly, the asymmetry of the LS profile, with respect to the b.c.p., is distinctly increased from HC to HF. This dependence could therefore provide a clear and sensitive indicator of the increased asymmetry and polar character of a bond along a series or in different chemical environments. This indicator could also be useful for assessing the characteristics and performance of the radial functions to be used in multipole models for X-ray structure-factor refinement. Reproducing the LS asymmetry with respect to the b.c.p. could be used as an alternative, particularly sensitive and suitable constraint when defining the optimal expansion–contraction coefficients k in double-zeta multipole refinements (Volkov & Coppens, 2001), adopting, for instance, the Hansen–Coppens formalism (Coppens, 1997). In their study, Volkov & Coppens (2001) used the profile of the charge density along the bond path to define an agreement factor between the theoretical charge-density refinement and the charge density from multipole refinement of the theoretical structure factors, and so obtain the optimal radial functions for different bond types.

The trend of the LS profile asymmetry from HB to HF would suggest that the source function contribution from the H atom to the density at the b.c.p. increases not only in absolute value but also in percentage along this series. If we look at the S(b.c.p., H)% values in Table 1 we see that just the opposite is true, since the t intervals excluded from the plot reverse the relative weight of the H and *X* contributions in the $(t_{\rm b.c.p.} - 0.2) \leq t \leq (t_{\rm b.c.p.} + 0.2)$ interval. Indeed, as explained by Gatti *et al.* (2003), the trend of S(b.c.p., H)% values in Table 1 agrees with the increased electronegativity of *X* along the series. In Fig. 1, we report LS profiles just around the b.c.p., not because this is necessarily the most representative interval of the whole source contributions from the bonded atoms, but to show how the contribution profiles of these atoms differ from one another in their outermost valence regions along the bond.

We analyse now the LG and LV contributions to LS. The local source LS would vanish everywhere for a uniform density distribution, one for which the Laplacian is always zero and $2G = -V$ everywhere.[4] This is not the case of an

[4] In this case the system is not bounded and the constant electron density at any point **r** may be seen as arising from the flux, through the surface boundary of a region containing the point, of the electric field density at **r** due to the density on the surface (Bader & Gatti, 1998).

Table 2
Prototypical DHA bonds: properties and source function contributions at the hydrogen-bond c.p. ($\mathbf{r}_b$).

All quantities are in a.u. unless otherwise stated.

System	Bond class†	$R_{D\cdots A}$ (Å)	$\rho(\mathbf{r}_b)$	$\nabla^2\rho(\mathbf{r}_b)$	$G(\mathbf{r}_b)$	$V(\mathbf{r}_b)$	S(H)	S(H)%‡	$S(D)$%‡	$S(A)$%‡	S(H+D+A)%‡
I	+CAHB	2.409	0.167	−0.415	0.084	−0.272	0.052	31.4	9.6	51.7	92.7
II	−CAHB	2.430	0.167	−0.392	0.085	−0.268	0.053	32.1	8.3	49.9	90.3
III	RAHB	2.538	0.056	0.148	0.042	−0.046	0.001	2.1	34.7	34.0	70.8
IV	PAHB	2.749	0.035	0.092	0.025	−0.027	−0.005	−14.4	53.1	31.0	69.7
V	IHB	2.876	0.029	0.076	0.021	−0.022	−0.007	−23.2	63.5	29.4	69.7
VI	IHB	3.199	0.020	0.048	0.013	−0.015	−0.004	−21.7	35.7	22.0	36.0

† Gilli & Gilli (2000) ‡ Percentage source contributions to the density at the hydrogen-bond c.p. from the atoms reported in parentheses. D is the donor and A the acceptor atom.

atomic distribution where the dominant role of the attractive force exerted by the nucleus imparts a form to the electron distribution and gives rise to the alternating presence of spherical shells of excess potential energy density [$2G(\mathbf{r}) < -V(\mathbf{r})$] and excess kinetic energy density [$2G(\mathbf{r}) > -V(\mathbf{r})$]. Furthermore, when atoms combine with one another in a molecule, the binding forces impart further structure to the system, by distorting to a greater or lesser extent the atomic spherical shell structure and the associated regions of excess potential or kinetic energy density. The modest LS contributions to the density from regions close to the b.c.p. in HLi and HBe (Fig. 1*a*) are the result of the very low G and V values (Table 1) and consequently LG and LV contributions. Since electrons have in this region an excess kinetic energy, in agreement with the non-shared character of the interaction, the LS contribution turns out to be negative and with higher magnitudes on the X side, especially for X = Be. For HB, the electrons around the b.c.p. start to have, on average, lower velocities than those implied by the local potential energy and therefore supply electron density at the b.c.p., instead of removing it from this point. At $t = 0.61$, the Laplacian becomes positive, the local source becomes negative and LG dominates over LV. The local source contributions LS from HC to HF are much larger than those in HLi and HBe and, in particular, are proportionally much larger compared with the corresponding values for the density at the b.c.p. This fact is the result of the dominance of the LV term, which closely follows from above the LS curve in these molecules. Indeed, it is the shape of the source contribution related to the potential energy density that imparts to the LS curves the characteristic increasing asymmetry with respect to the b.c.p. with increasing electronegativity of X. The situation is reversed with respect to HLi and HBe, where it is the sink contribution related to the kinetic energy that mostly imparts a form to the local source LS. In conclusion, significant positive source contributions from regions around the b.c.p. are to be expected only for those shared bonds where the LV term is dominating and charge is being accumulated along the bond, whilst for those non-shared bonds in which the LG term dominates, modest and negative source contributions associated with charge removal from the internuclear region are to be anticipated. This result is obviously in line with the usual analysis of the Laplacian portrait along these two extreme types of bonds. The LS, LG and LV profiles magnify these effects and those due to asymmetric sharing. Furthermore, on the one hand, these profiles refer to a well defined point (b.c.p.), with the advantage of focusing on a choice that does not favour one of the two interacting partners. On the other hand, by taking into account the remaining points along the bond, the study of these profiles avoids the disadvantages of restricting the analysis to just one given point. In a sense, this analysis adds to and detracts from the importance of the b.c.p. at the same time.

4.2. Prototypical hydrogen bonds.

Fig. 2 shows profiles for the electron density, its Laplacian, and the local source contributions LS, LG and LV for five prototypical O—H···O hydrogen bonds. Also shown are profiles for the case of the water–acetylene complex **VI**, a C—H···O hydrogen bond. Profiles are reported as a function of the dimensionless parameter t, with the H atom at $t = 0$ and the acceptor atom at $t = 1$. For each system, the interval $0.1 \leq t \leq 0.8$ is shown and the electron density is multiplied by a factor of 5 so as to report all quantities on the same scale. Table 2 lists various properties at the b.c.p. and the source contribution from the H atom to the electron density at the b.c.p. The percentage source contribution from the H atom, S(H)%, appears as a very distinctive marker of the hydrogen-bond strength in the O—H···O series. This parameter is highly negative for isolated hydrogen bonds, slightly negative for polarized-assisted hydrogen bonds, close to zero for resonance-assisted hydrogen bonds and largely positive for charge-assisted hydrogen bonds. The percentage source contribution from the H-atom donor D increases with increasing O···O separation and decreasing D—H distance, in agreement with the increased covalent and local character of the D—H bond. The source from the acceptor atom A shows, as expected, the opposite trend. The sum of percentage source contributions from the H atom, the H-atom donor and the H-atom acceptor, S(H+D+A)%, decreases with decreasing hydrogen-bond strength, consistent with the parallel increased electrostatic character of the interaction. However, **III**, **IV** and **V** have similar S(H+D+A)% values, despite having different $R_{D\cdots A}$ values; this outcome is probably due to an increased participation of atoms other than H, D and A in **IV** and particularly in **III**, as a result of resonance (**III**) or induction (**IV**) cooperative effects. For a thorough analysis of these points, see Gatti *et al.* (2003).

The profiles of the local sources for **I**–**VI** show that in the $0.1 \leq t \leq 0.75$ interval LS is everywhere positive for the strong charge-assisted hydrogen bonds **I** and **II**, while LS is close to zero for **V** and **VI**, except for the negative spike around the b.c.p. The case of the resonance-assisted hydrogen bond, **III**, and in part that of the polarized-assisted hydrogen bond, **IV**, is

borderline. In these systems, there are regions close to the H nucleus and to the acceptor atom that contribute significantly to accumulating density at the b.c.p., while the electron charge removal at the b.c.p. from regions close to this point is far more efficient than it is in **V** and **VI**. All these features agree with the trend of S(H)% values along the series. The positive Laplacian and negative LS values at the b.c.p. in **III**, whose magnitudes are larger than those in **IV**–**VI**, do not imply a negative S(H)% for this RAHB system because of the dominant positive source contributions from the remaining regions of the H-atom basin. The width of the peak around the b.c.p. for **I**–**VI** decreases with decreasing hydrogen-bond strength and increasing H$\cdots A$ distance, be this peak either positive or negative. This trend would definitely persist even if the H$\cdots A$ distance had not been normalized to one in the plots. This result implies that the magnitude of sources from points close to the b.c.p. decreases along the series. The LS profiles for **I**–**VI** confirm that the magnitudes of sources are limited from regions where the contribution related to the kinetic energy density dominates over that due to the potential energy density. This is the case for **V** and **VI**, the isolated hydrogen bonds, and in part for **IV**.

The LS profiles along the H$\cdots A$ interactions reveal interesting and characteristic features for all types of prototypical bonds. However, the profiles do not appear to discriminate clearly between **III** and **IV**, *i.e.* between RAHB and PAHB, although these systems exhibit different S(H)% values and *a fortiori* different S(H) values. Nor do the LS profiles appear to distinguish plainly between the two different types of IHBs, although these have different donor-to-acceptor separations. Systems **V** and **VI** have, indeed, a reversed trend for S(H)% and *a fortiori* for S(H), which is 30% less negative in **VI**. A more complete inspection of the local source contributions is needed in order to handle these cases. Figs. 3 and 4 detail the

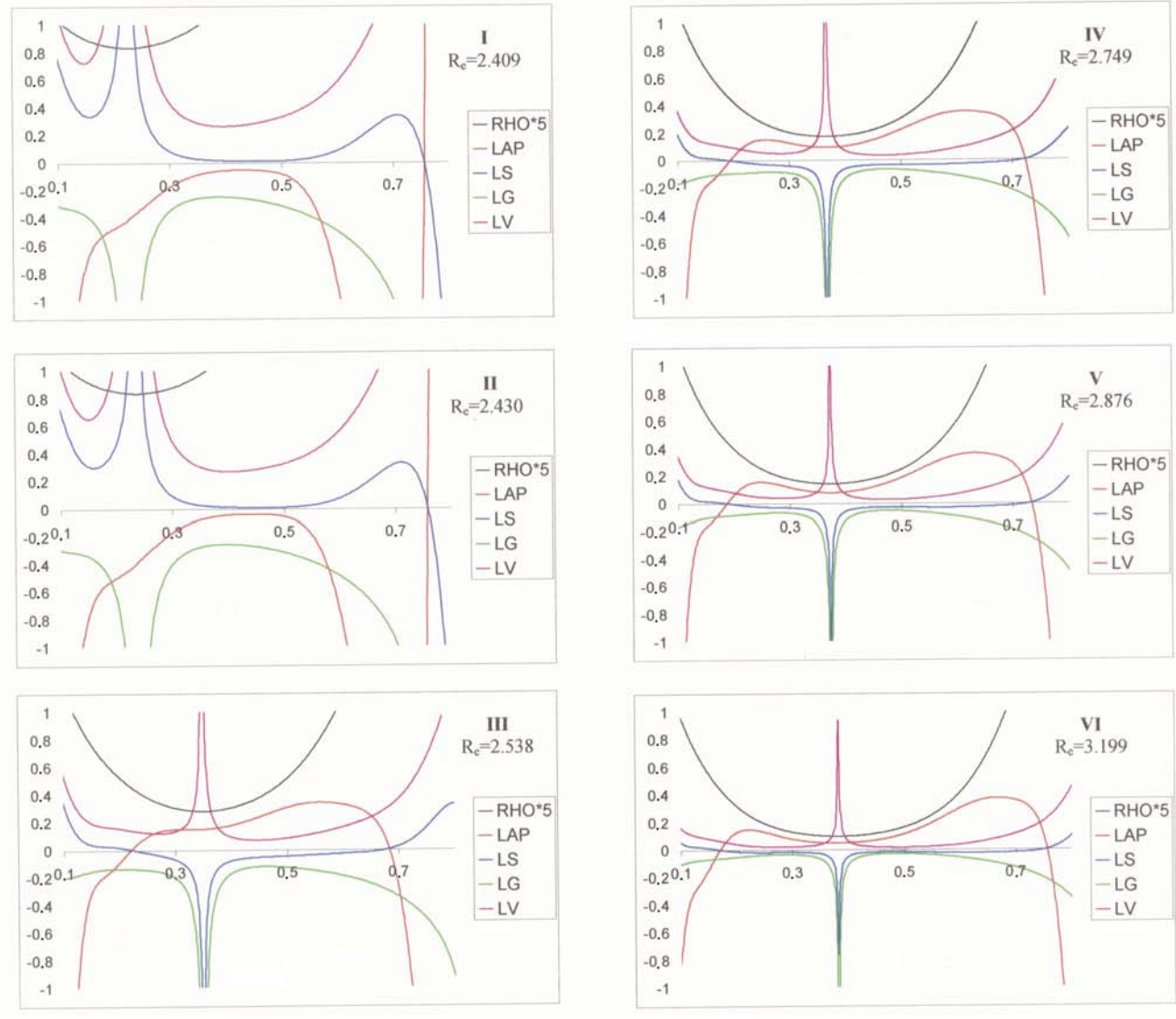

Figure 2
Prototypical hydrogen bonds. The local source contribution (LS) to the density at the b.c.p. from points lying on the bond path (t = 0 at the H atom and t = 1 at the O acceptor). The LG and LV components of LS and the profiles of the electron density (RHO) and Laplacian (LAP) are also reported. RHO is multiplied by 5 and all quantities are in a.u. (see text).

LS, LG and LV profiles for the densities at the hydrogen-bond critical points along the juxtapositions of the O—H (or C—H for **VI**) and H···O bond paths for all these systems. Profiles are here reported as a function of X, with X being a running coordinate, in Å, along the two combined bond paths and with the donor atom at $X = 0$. The electron density profiles in Fig. 3 allow the boundaries for the H-atom basin to be determined. It is clear that the reason why the source is greater in **III** than in **IV** is mostly because of the 10–15% increase of the positive LS (and LV) peak around the H nucleus. This increase overcomes the higher negative source contributions of **III** in the hydrogen-bond region. When comparing **V** and **VI**, we would expect a less negative S(H) value in **V** than in **VI** because of the higher positive peak of LS close to the H nucleus. This is not the case. Indeed, the greater polarization of the O—H bond with respect to the C—H bond brings the O—H b.c.p. much closer to the H nucleus in **V** than in **VI**, thereby removing from the H basin most of the tail, closer to the donor atom, of the positive LS peak surrounding the H nucleus. This removal prevails over the increase of S(H) due to the higher positive peak around the H nucleus, yielding to a more negative S(H) value in **V** than in **VI**. The shift of the b.c.p. towards the donor atom in the C—H interaction leads, in turn (Table 2), to a decrease of the source from the donor atom, instead of the expected increase, on passing from **V** to **VI**.

The local source contributions to the density at the hydrogen-bond c.p. emphasize the importance of the overall charge-density polarization occurring to the atoms involved in the hydrogen bond. This polarization must be different for C—H···O and O—H···O bonds, even if at similar donor-to-acceptor separations these bonds would exhibit similar features at their hydrogen-bond c.p.s as a result of their differently shaped LS contributions having similar averages. Espinosa *et al.* (1998) have pointed out that the H···O distance summarizes the essential features of the hydrogen-bond interaction, with G, V and λ_3 values at the hydrogen-bond c.p. being correlated and decaying exponentially with such a distance. A much less satisfactory correlation was found for ρ_b (Espinosa *et al.*, 1999). This might be an indication that, while G, V and λ_3 are primarily functions of the H···O distance only, ρ_b has, on the contrary, a more complex dependence on the overall charge-density polarization due to hydrogen-bond formation. Indeed, for weak interactions, the G, V and λ_3 values of promolecular and crystalline distributions are very much alike (Spackman, 1999; Gatti *et al.*, 2002) and therefore do not provide much additional information

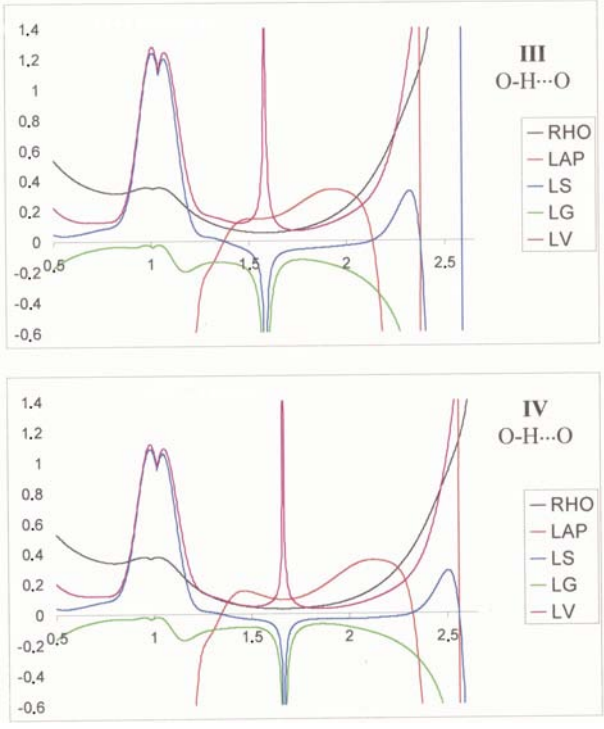

Figure 3
Local source contribution profiles along the juxtaposition of O—H and H···O bond paths for a prototypical RAHB (malonaldeyde, **III**) and a PAHB (cyclic trimer of water, **IV**). The contributions refer to the hydrogen-bond critical point. Values on the abscissa are in Å, with $x = 0$ at the donor atom. The H-atom boundaries are visible from the electron density (RHO) profile and the positive spike of the local source contribution at the hydorgen-bond c.p. All quantities are in a.u., except for the coordinate along the bond paths.

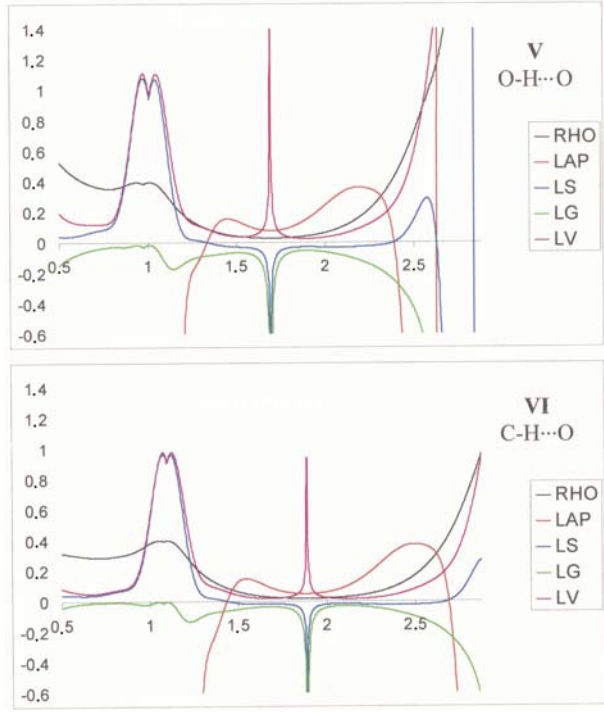

Figure 4
Local source contribution profiles along the juxtaposition of D—H and H···O bond paths for prototypical O—H···O (linear water dimer, **V**) and C—H···O bonds (acetylene–water linear complex, **VI**). The contributions refer to the hydrogen-bond critical point. Values on the abscissa are in Å, with $x = 0$ at the donor atom. The H-atom boundaries are visible from the electron density (RHO) profile and the positive spike of the local source contribution at the hydrogen-bond c.p. All quantities are in a.u., except for the coordinate along the bond paths.

Table 3
Hydrogen-bond c.p. properties for the shortest (H···O = 1992 Å) N—H···O bond in the urea crystal.

Data are for the crystal density, the model density of non-interacting molecules positioned as in the crystal and the density of the independent atom model. All quantities are in a.u. unless otherwise stated.

Electron density	R_H (Å)†	$\rho(\mathbf{r}_b)$	$\nabla^2\rho(\mathbf{r}_b)$	$G(\mathbf{r}_b)$	$V(\mathbf{r}_b)$
Crystal	0.700	0.0223	0.0705	0.0182	−0.0187
Superposition of molecules	0.720	0.0220	0.0713	0.0177	−0.0177
Superposition of atoms (IAM)	0.808	0.0293	0.0798	0.0202	−0.0205

† Hydrogen-bond c.p. distance from H nucleus.

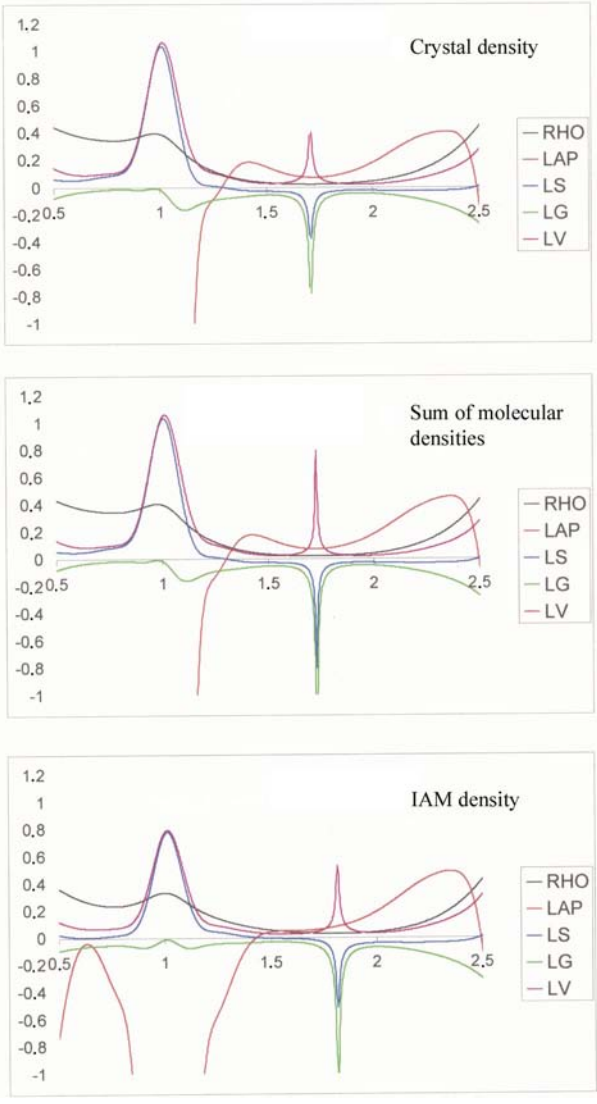

Figure 5
The electron density, Laplacian and local source contributions for the shorter N—H···O hydrogen bond in crystalline urea, as a function of the adopted electron density (see text). Profiles are shown along the juxtaposition of N—H and H···O bond paths. The local source contributions refer to the hydrogen-bond critical point. Values on the abscissa are in Å, with $x = 0$ at the N nucleus. The H-atom boundaries are visible from the electron density (RHO) profile and the positive spike of the local source contribution at the hydrogen-bond c.p. All quantities are in a.u., except for the coordinate along the bond paths.

about these intermolecular interactions. On the contrary, the LS profiles and the source function analysis should add specific information about these interactions manifested in the changes in the H-atom population, atomic moment and volume induced by hydrogen-bond formation. These latter quantities have been proposed as valuable criteria for establishing the existence of hydrogen bonds in gas (Koch & Popelier, 1995) and crystalline phases (Gatti *et al.*, 2002).

4.3. Deformation density, interaction density and the local source contributions.

Fig. 5 displays profiles for the electron density, its Laplacian, and the local source contributions LS, LG and LV for the shorter (H···O = 1.992 Å) of the two unique N—H···O hydrogen bonds in crystalline urea. The local source contributions refer to the hydrogen-bond critical point and profiles are shown along the juxtaposition of N—H and H···O bond paths, so as to emphasize the source contributions from the whole H-atom basin. Profiles in Fig. 5 have been evaluated using three different densities: the crystal density (top), the model density (middle) of non-interacting molecules positioned as in the crystal and the model density (bottom) of non-interacting atoms (IAM model). Table 3 lists the corresponding hydrogen-bond critical point properties. On passing from the IAM model to the superposition of molecules and then to the crystal density, the hydrogen-bond critical point moves towards the H nucleus (Fig. 5 and Table 3). As expected, the profiles for the source contributions from the IAM model show the largest deviations with respect to the contributions from the crystal density. The largest difference concerns the shape and height of the LS and LV wide positive peaks around the H nucleus. These peaks are more symmetric and about 25% lower for the IAM density compared with the profiles for the crystal density. Also noticeable is the difference in the shape of the LS peak around the hydrogen-bond critical point. The LS peak is asymmetric in the IAM density, while it is much less so for the other two densities, as a result of a more symmetric Laplacian distribution around the b.c.p. in the latter. Fig. 6 displays the differences in the profiles of the density and of its Laplacian for the crystal density with respect to the two adopted model densities. The regions close to the hydrogen-bond critical point (between 1.6 and 2.0 Å; Fig. 6) are those in which these differences are at a minimum for both model densities. *It appears that the properties at the hydrogen-bond critical point and in the region close to it contain the least information* – when compared with other regions of the H basin – *on the electron-density polarization due to intermolecular interactions* (or to the combination of intra- and intermolecular interactions in the case of difference with the IAM density). This observation raises serious doubts about the use of the b.c.p. properties only when discussing intermolecular interactions in crystals, as pointed out recently by Gatti *et al.* (2002), albeit at a qualitative level only. Fig. 7 shows differences of the local source contributions to the density at the hydrogen-bond critical point between the crystal density and each of the two adopted model densities. As reference

point for evaluating LS, LG and LV, we assumed the hydrogen-bond critical point of the crystal density. It is clear that the largest differences in the local source contributions to the density at the hydrogen-bond critical point occur far from this point, in a region close to the H nucleus and encompassing a large portion of the H basin. Differences between the crystal density and the superposition of molecular densities are one order of magnitude lower than those for the IAM density and display opposite profiles along the N—H and O···H bond paths, within the H basin. The LS contributions along the N—H bond are higher for the crystal density than for the IAM density, while they are generally lower along the hydrogen bond and starting at ∼0.1 Å from the H nucleus. An LS difference of 0.1 a.u. at 1 a.u. from the reference point (Fig. 7, top) implies a local $|\nabla^2\rho|$ difference of about 1.3 a.u. (31 e Å^{-5}), which is certainly amenable to experimental determination. Such is typically the case for the IAM *vs* the crystal density source contributions. The interaction density effects are much lower (Fig. 7, bottom) and an LS difference of 0.02 a.u. at 1 a.u. from the reference point would imply a local $|\nabla^2\rho|$ difference of about 0.3 a.u. (6 e Å^{-5}). Although significantly lower than for the case of the IAM density, this difference should also be amenable to experimental determination (Destro *et al.*, 2000). The trend of the difference profiles around the H nucleus reported in Fig. 7 should be *a fortiori* experimentally detectable. This situation contrasts with the differences observed for the $\rho(r_b)$ and the $\nabla^2\rho$ values at the hydrogen-bond critical point between the crystal density and the two model densities (Table 3). These differences are probably below or at the limit of experimental determination (Krijn *et al.*, 1988; Destro *et al.*, 2000). Recently, Spackman *et al.* (1999) studied the effects of intermolecular interactions, especially hydrogen bonding, on the electron density in a crystal and the observable structure factors. By analysing systematically the structure-factor differences between the crystal density and the superimposed molecular densities, Spackman *et al.* (1999) were able to conclude that the interaction density is not a random effect but rather a systematic one, which should therefore be amenable to observation under proper conditions. The regularity of the profiles shown in Fig. 7 is another demonstration that the interaction density is not a random effect. The analysis of these profiles could be an interesting and alternative way to gain an insight, in real space, into the effects of intermolecular interactions. When combined with a theoretical analysis, the study of the LS profiles (and differences) could help in assessing whether the data quality of a given experimental determination allows for a meaningful study of the intermolecular interaction effects. This use of the LS function will be explored in further studies. On the one hand, one would be focusing on the electron-density value at the intermolecular b.c.p., which represents the

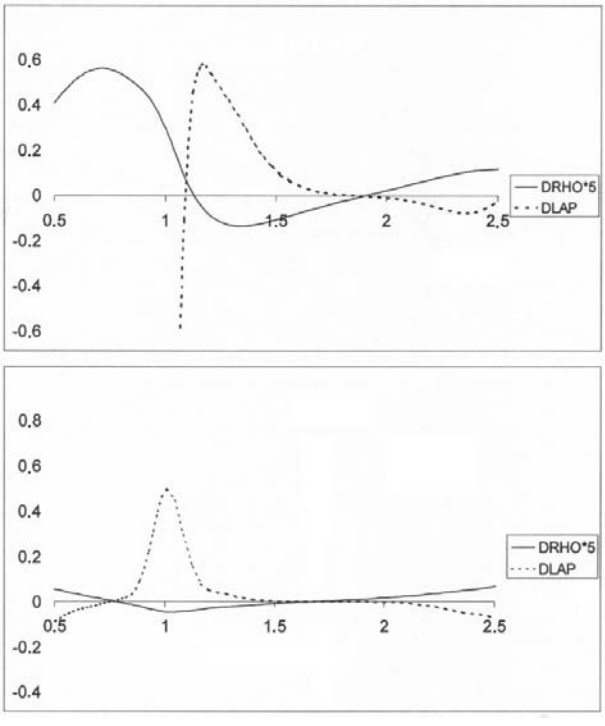

Figure 6
Differences DX (X = RHO and LAP) for the shorter N—H···O hydrogen bond in crystalline urea. Top: crystal density–IAM model density. Bottom: crystal density–superposition of molecular densities. Profiles are shown along the juxtaposition of N—H and H···O bond paths. Values on the abscissa are in Å, with $x = 0$ at the N nucleus. All quantities are in a.u., except for the coordinate along the bond paths.

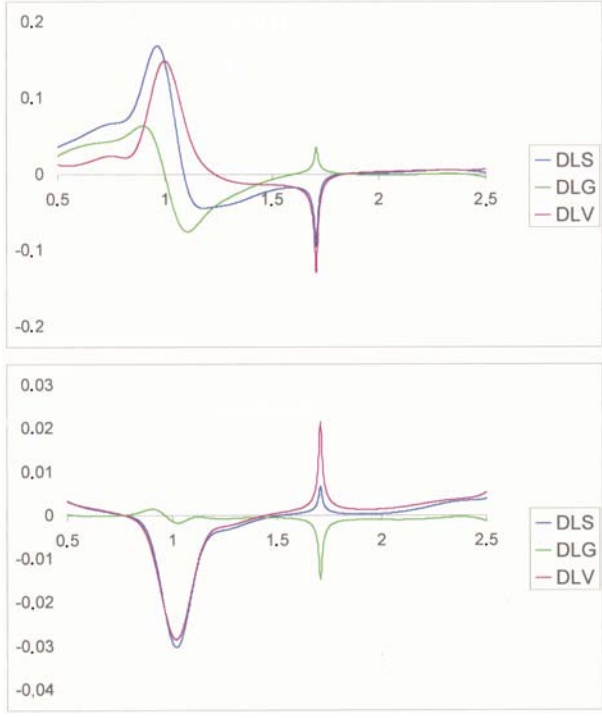

Figure 7
Differences DX (X = LS, LV and LG) in the local source contributions for the shorter N—H···O hydrogen bond in crystalline urea. Top: crystal density–IAM model density. Bottom: crystal density–superposition of molecular densities. Profiles are shown along the juxtaposition of N—H and H···O bond paths. The local source contribution differences refer to the hydrogen-bond critical point (coordinates of the crystal density). Values on the abscissa are in Å, with $x = 0$ at the N nucleus. All quantities are in a.u., except for the coordinate along the bond paths.

least biased choice but which is also known to be intrinsically poorly informative about the intermolecular interaction. On the other hand, one would be analysing at the same time how this specific electron-density value results from a charge-density rearrangement encompassing the whole space.

5. Final remarks

This paper has addressed the question of whether the analysis of the local source contributions to the electron density at a point is interesting in its own right, as is the study of the condensed-to-atom form of these contributions. To answer this question, we state the following.

(*a*) The analysis of the local source profiles along a bond path provides an interesting fingerprint of a given bonding interaction, especially so if a series of related chemical bonds is considered and if the contributions related to the kinetic energy and potential energy densities are also scrutinized. The asymmetry of the LS profile, with respect to the b.c.p., appears as a very sensible indicator of the extent of the polar character of a shared bonding interaction. As such, this profile could perhaps be used as an aid in selecting the optimal radial functions in the multipolar analysis of X-ray diffraction data.

(*b*) The investigation of the local source contributions to the density at the hydrogen-bond c.p. enlightens and emphasizes the role of the overall charge-density polarization occurring to the atoms involved in the hydrogen bond. This result raises doubts about the use of the b.c.p. properties only when discussing intermolecular interactions in crystals.

(*c*) Deformation densities and interaction densities generally reach absolute minimum values in regions close to the hydrogen-bond critical point. Local contributions to the density at this point clearly show that the largest differences in these contributions due to intramolecular bonding and crystallization occur far from the b.c.p. and in regions encompassing large portions of the H basin. Analysis of the differences of local source contributions between the crystal density and the superimposed molecular density enables us to reveal, in real space, the effects of intermolecular interactions whilst referring to a point that represents the least biased choice for a given interaction.

References

Abramov, Yu. A. (1997). *Acta Cryst.* A**53**, 264–272.

Arfken, G. (1985). *Mathematical Methods for Physicists*, pp. 897–898. Orlando, Florida: Academic Press.

Bader, R. F. W. (1990). *Atoms in Molecules. A Quantum Theory. International Series of Monographs on Chemistry* 22. New York: Oxford University Press.

Bader, R. F. W. & Gatti, C. (1998). *Chem. Phys. Lett.* **287**, 233–238.

Cleland, W. W. & Krevoy, M. M. (1994). *Science*, **264**, 1887–1890.

Coppens, P. (1997). *X-ray Charge Densities and Chemical Bonding. IUCr Texts on Crystallography* No. 4. IUCr/Oxford University Press.

Cremer, D. & Kraka, E. (1984). *Croat. Chem. Acta*, **57**, 1259–1281.

Destro, R., Roversi, P., Barzaghi, M. & Marsh, R. E. (2000). *J. Phys. Chem. A*, **104**, 1047–1054.

Dyke, T. R., Mack, K. M. & Muenter, J. S. (1977). *J. Chem. Phys.* **66**, 498–510.

Espinosa, E., Molins, E. & Lecomte, C. (1998). *Chem. Phys. Lett.* **285**, 170–173.

Espinosa, E., Souhassou, M., Lachekar, H. & Lecomte, C. (1999). *Acta Cryst.* B**55**, 563–572.

Frisch, M. J., Trucks, G. W., Schlegel, H. B., Scuseria, G. E., Robb, M. A., Cheeseman, J. R., Zakrzewski, V. G., Montgomery, J. A., Stratmann, R. E., Burant, J. C., Dapprich, S., Millam, J. M., Daniels, D. A., Kudin, K. N., Strain, M. C., Farkas, O., Tomasi, J., Barone, V., Cossi, M., Cammi, R., Mennucci, B., Pomelli, C., Adamo, C., Clifford, S., Ochterski, J., Petersson, G. A., Ayala, P. Y., Cui, Q., Morokuma, K., Malick, D. K., Rabuck, A. D., Raghavachari, K., Foresman, J. B., Cioslowski, J., Ortiz, J. V., Stefanov, B. B., Liu, G., Liashenko, A., Piskorz, P., Komaromi, I., Gomperts, R., Martin, R. L., Fox, D. J., Keith, T., Al-Laham, M. A., Peng, C. Y., Nanayakkara, A., Gonzalez, C., Challacombe, M., Gill, P. M. W., Johnson, B. G., Chen, W., Wong, M. W., Andres, J. L., Head-Gordon, M., Replogle, E. S. & Pople, J. A. (1998). *GAUSSIAN98*, Revision A.1. Gaussian Inc., Pittsburgh, PA, USA.

Fuster, F. & Silvi, B. (2000). *Theor. Chem. Acc.* **104**, 13–21.

Gatti, C. (1999). *TOPOND98. An Electron Density Topological Program for Systems Periodic in N (N = 0–3) Dimensions.* CNR–ISTM, Milan, Italy.

Gatti, C., Cargnoni, F. & Bertini, L. (2003). *J. Comput. Chem.* **24**, 422–436.

Gatti, C., Fantucci, P. & Pacchioni, G. (1987). *Theor. Chim. Acta*, **72**, 433–458

Gatti, C., May, E., Destro, R. & Cargnoni, F. (2002). *J. Phys. Chem. A*, **106**, 2707–2720.

Gatti, C., Saunders, V. R. & Roetti, C. (1994). *J. Chem. Phys.* **101**, 10686–10696.

Gilli, G. & Gilli, P. (2000). *J. Mol. Struct.* **552**, 1–15.

Hô, M., Smith, V. H. Jr, Weaver, D. F., Gatti, C., Sagar, R. P. & Esquivel, R. O. (1998). *J. Chem. Phys.* **108**, 5469–5475.

Huber, K. & Herzberg, G. (1979). *Molecular Spectra and Molecular Structure*, Vol. IV, *Constants of Diatomic Molecules.* New York: Van Nostrand Reinhold.

Jayatilaka, D. & Grimwood, D. J (2001). *Acta Cryst.* A**57**, 76–86.

Jeffrey, G. A. (1997). *An Introduction to Hydrogen Bonding.* New York: Oxford University Press.

Koch, U. & Popelier, P. L. A. (1995). *J. Phys. Chem.* **99**, 9747–9754.

Krijn, M. P. C. M., Graafsma, H. & Feil, D. (1988). *Acta Cryst.* B**44**, 609–616.

McMaster University (1997). *AIMPAC.* McMaster University, Ontario, Canada.

Mó, O., Yáñez, M. & Elguero, J. J. (1992). *Chem. Phys.* **97**, 6628–6638.

Overgaard, J., Schiøtt, B., Larsen, F. K. & Iversen, B. B. (2001). *Chem. Eur. J.* **7**, 3756–3767.

Pan, Y. & McAllister, M. A. (1997). *J. Am. Chem. Soc.* **119**, 7561–7566.

Saunders, V. R., Dovesi, R., Roetti, C., Causà, M., Harrison, N. M., Orlando, R. & Zicovich-Wilson, C. M. (1998). *CRYSTAL*98 *User's Manual.* University of Turin, Italy.

Spackman, M. A. (1999). *Chem. Phys. Lett.* **301**, 425–429.

Spackman, M. A., Byrom, P. G., Alfredsson, M. & Hermansson, K. (1999). *Acta Cryst.* A**55**, 30–47.

Swaminathan, S., Craven, B. M. & McMullan, R. K. (1984). *Acta Cryst.* B**40**, 300–306.

Turi, L. & Dannenberg, J. J. (1993). *J. Phys. Chem.* **97**, 7899–7909.

Volkov, A. & Coppens, P. (2001). *Acta Cryst.* A**57**, 395–405.